crystals

MDPI

Article

Deconvolution of the MBP-Bri2 Interaction by a Yeast Two Hybrid System and Synergy of the AlphaFold2 and High Ambiguity Driven Protein-Protein Docking

Evgeniya V. Smirnova [1], Tatiana V. Rakitina [1], George A. Saratov [1,2], Anna A. Kudriaeva [1] and Alexey A. Belogurov, Jr. [1,3,*]

[1] Shemyakin-Ovchinnikov Institute of Bioorganic Chemistry, Russian Academy of Sciences, 117997 Moscow, Russia; smirnova.evgeniya@gmail.com (E.V.S.); taniarakitina@yahoo.com (T.V.R.); saratov.ga@phystech.edu (G.A.S.); anna.kudriaeva@gmail.com (A.A.K.)

[2] Moscow Institute of Physics and Technology, National Research University, 141701 Dolgoprudny, Moscow Region, Russia

[3] Department of Biological Chemistry, Evdokimov Moscow State University of Medicine and Dentistry, 127473 Moscow, Russia

* Correspondence: belogurov@ibch.ru; Tel.: +7-(495)-3366166

Abstract: Myelin basic protein (MBP) is one of the key proteins in the development of multiple sclerosis (MS). However, very few intracellular MBP partners have been identified up to now. In order to find proteins interacting with MBP in the brain, an expression library from the human brain was screened using a yeast two-hybrid system. Here we showed that MBP interacts with the C-terminal 24-residue peptide of Integral transmembrane protein II associated with familial British and Danish dementia (ITM2B/Bri2 or Bri2). This peptide (Bri23R) was one residue longer than the known Bri23 peptide, which is cleaved from the C-terminus of Bri2 during its maturation in the Golgi and has physiological activity as a modulator of amyloid precursor protein processing. Since the spatial structures for both MBP and Bri2 were not known, we used computational methods of structural biology including an artificial intelligence system AlphaFold2 and high ambiguity driven protein-protein docking (HADDOCK 2.1) to gain a mechanistic explanation of the found protein-protein interaction and elucidate a possible structure of the complex of MBP with Bri23R peptide. As expected, MBP was mostly unstructured, although it has well-defined α-helical regions, while Bri23R forms a stable β-hairpin. Simulation of the interaction between MBP and Bri23R in two different environments, as parts of the two-hybrid system fusion proteins and in the form of single polypeptides, showed that MBP twists around Bri23R. The observed interaction results in the adjustment of the size of the internal space between MBP α-helices to the size of the β-hairpin of Bri23R. Since Bri23 is known to inhibit aggregation of amyloid oligomers, and the association of MBP to the inner leaflet of the membrane bilayer shares features with amyloid fibril formation, Bri23 may serve as a peptide chaperon for MBP, thus participating in myelin membrane assembly.

Keywords: myelin basic protein; MBP; integral transmembrane protein II associated with familial British and Danish dementia; ITM2B/Bri2; two hybrid system; β-hairpin; AlphaFold2; molecular docking; HADDOCK

check for updates

Citation: Smirnova, E.V.; Rakitina, T.V.; Saratov, G.A.; Kudriaeva, A.A.; Belogurov, A.A., Jr. Deconvolution of the MBP-Bri2 Interaction by a Yeast Two Hybrid System and Synergy of the AlphaFold2 and High Ambiguity Driven Protein-Protein Docking. *Crystals* **2022**, *12*, 197. https://doi.org/10.3390/cryst12020197

Academic Editor: Abel MORENO

Received: 30 November 2021
Accepted: 24 January 2022
Published: 28 January 2022

Publisher's Note: MDPI stays neutral with regard to jurisdictional claims in published maps and institutional affiliations.

Copyright: © 2022 by the authors. Licensee MDPI, Basel, Switzerland. This article is an open access article distributed under the terms and conditions of the Creative Commons Attribution (CC BY) license (https://creativecommons.org/licenses/by/4.0/).

1. Introduction

In 1971, the structural biology community established the single worldwide archive for macromolecular structure data—the Protein Data Bank (PDB). Today, hundreds of data resources and millions of researchers, which explore fundamental biology and biomedicine, use PDB. The tremendous amount of structural information collected over 50 years was used in the creation and testing of AlphaFold2—an artificial intelligence system developed by DeepMind (https://deepmind.com, accessed on 10 October 2021) to predict the spatial

structure of proteins based on amino acid sequence [1–4]. This artificial neural network is based on the so-called "attention" approach. Attention is a way to tell the network what to pay more attention to, that is, to report the probability of a particular outcome depending on the state of the neurons and the input data [5]. The identification of important factors is carried out through the method of backpropagation of the error [6]. It should be noted that the previous advances in structural biology and, above all, protein crystallography, made it possible to obtain more than 170 thousand spatial structures of proteins, on which AlphaFold2 was trained [3]. Several reports have shown that the accuracy of predicting the spatial structures of proteins in most cases is not inferior to the experimentally obtained structures [7], and in some cases, it gives the same quality as the crystal structure obtained at a resolution of 1.1 Å [7]. This fact opens significant opportunities for both fundamental and applied biological and pharmacological research [8,9]. It is obvious that AlphaFold2 is most in demand when working with the proteins that are most difficult for direct structural study, which include intrinsic disordered proteins (IDP) and their interaction networks [10].

Myelin basic proteins (MBPs) are the key proteins in the development of neurodegenerative diseases including multiple sclerosis (MS), which are form a family of many members whose expression is regulated by developmental stage, choice of transcription initiation point, differential splicing, and post-translational modifications [11–16]. The "classic" isoform of MBP is a protein with a molecular weight of 18.5 kDa, which predominates in myelin in adults and provides condensation of the mature myelin sheath in the central nervous system, thus maintaining its structural integrity. MBPs are associated with the membrane, and they have also been shown to interact with a number of other proteins, including structural proteins (actin and tubulin), signaling proteins (Ca(2+)-calmodulin) and proteins containing SH3-domain [17–20]. The updated description of the MBP interacting network is reported in Smirnova et al. [21]. MBPs have an intrinsically disordered structure, which is an excellent matrix for numerous protein-protein interactions, and further undergo various post-translational modifications, including methylation, phosphorylation, and deamination [22].

Despite the critical role of MBP in the functioning of the nervous system, and the large volume of research conducted in the field of search for proteins interacting with MBP, only a small fraction of MBP interacting partners have been thoroughly investigated. Many of the in vitro methods widely used to identify protein-protein interactions, such as pulldown or immunoprecipitation, are not suitable for MBP due to the low compatibility with the conformational variability of IDPs. One of the solutions is the use of in vivo methods for interaction studies, to which the yeast two-hybrid systems (Y2HS) belong [23,24]. These systems make it possible to analyze the interaction of proteins in the environment of a eukaryotic cell preserving post-translational protein modifications. However, the result obtained requires confirmation by an independent method. In some cases, computational approaches providing visualization and mechanistic explanation of the presumed protein-protein interaction may complement the Y2HS-based study.

In this work, the search for MBP-interacting proteins, using the Matchmaker Gold Yeast Two-Hybrid System identified the C-terminal 24-residue peptide of Integral transmembrane protein II associated with familial British and Danish dementia (ITM2B/Bri2 or Bri2). This peptide represents a β-hairpin that is proteolytically cleaved from the luminal domain of Bri2 in vivo. To obtain an insight into the MBP-Bri2 relationship, a combination of AlphaFold2 and docking program HADDOCK was applied to simulate the found interactions between MBP and the β-hairpin of Bri2 in two different protein environments: when they are parts of the fusion protein components of the Y2HS, as well as when free MBP interacts with free β-hairpin.

2. Materials and Methods

2.1. Cloning of MBP Bait Gene into pGBKT7 Vector

Full MBP fragment was amplified by PCR using primers GATATACATATGGCGTCTCAGAAGCGTC (MBP pGBKT7 fr) and AGCTCTCGAGTTATCAGCGACGAGCCATCGGA-

GAG (MBP pGBKT7 rev). PCR amplification of MBP-encoding sequence was performed through the following PCR program: 94 °C for 4 min, then 25 cycles each at 94 °C for 30 s/60 °C for 30 s/72 °C for 30 s, followed by incubation at 72 °C for 10 min and cooling to 4 °C. Vector plasmid pGBKT7 was digested using restriction enzymes NdeI and SalI (NewEnglandBiolabs, Ipswich, MA, USA), and MBP PCR fragment was digested using NdeI and XhoI (NewEnglandBiolabs, Ipswich, MA, USA). Both fragments were gel purified and ligated using T4 DNA ligase (ThermoScientific, Waltham, MA, USA). Ligate was transformed into XL-1 cells, which were spread onto kanamycin plates.

2.2. Preparation of Competent Yeast Cells

To prepare the yeast competent cells we followed the protocol provided with the Yeastmaker Yeast Transformation System 2 (Takara Bio USA, Inc., San Jose, CA, USA). Briefly, Y187 or Y2H strains from a frozen yeast stock were streaked on YPDA agar plates. The plates were incubated at 30 °C until colonies appeared (approximately 3 days). After that, one fresh 2–3 mm colony was inoculated into 3 mL of YPDA medium containing 50 μg/mL kanamycin in a sterile 15 mL culture tube. The tubes were incubated at 30 °C with shaking at 250 rpm for 8–12 h. Then the 5 μL of the culture were transferred to 50 mL of YPDA in a 250 mL flask, and the culture was incubated with shaking until the OD_{600} reached 0.3 (20 h). Then the cells were collected by centrifugation at 700 g for 5 min at room temperature. The pellet was resuspended in 100 mL of fresh YPDA and incubated at 30 °C until the OD_{600} reached 0.5 (3 h). The cells from the culture were collected at 700 g for 5 min at room temperature into two 50 mL sterile Falcon conical tubes resuspended in 30 mL sterile, deionized H_2O. The cells were again centrifuged at 700 g for 5 min at room temperature, the supernatant was discarded, and each pellet was resuspended in 1.5 mL of 1.1× TE/LiAc. Cell suspensions were transferred into 1.5 mL tubes, and the cells were pelleted at high speed for 15 s. Finally, each cell pellet was resuspended in 600 μL of 1.1× TE/LiAc, and that suspension was used for transformation with plasmid DNA.

2.3. Transformation of Yeast Cells

The transformation of yeast cells was performed according to the small-scale protocol provided with the Yeastmaker Yeast Transformation System 2 (Takara Bio USA, Inc., San Jose, CA, USA). Briefly, in a pre-chilled 1.5 mL tube, 100 ng of appropriate plasmid DNA was combined and mixed with 50 μg of denatured Yeastmaker Carrier DNA and 50 μL freshly prepared yeast competent cells. Then, 500 μL of PEG/LiAc was added to the plasmid/cells mixture. The resulting volume was gently mixed and incubated at 30 °C for 30 min with inverting the tube every 10 min. The 20 μL of DMSO was added to the volume and mixed by inverting the tube. Then the volume was gently incubated at 42 °C for 15 min with inverting the tube every 5 min. After incubation, the cells were collected by centrifugation at high speed for 15 s and resuspended into 1 mL of YPD Plus Medium, and the suspension was incubated at 30 °C for 30 min with shaking. The cells were collected by centrifugation at high speed for 15 s and resuspended into 1 mL of 0.9% NaCl solution. Then the cells were seeded to the appropriate selection media.

2.4. Obtaining of Control Mated Strains

To obtain control strains containing two plasmids, a procedure for mating yeast cells was performed. One colony for each individual strain to mate was selected for use in the mating procedure. Both colonies were placed in one 1.5 mL centrifuge tube containing 500 μL of 2× YPDA and vortexed. The mixture was incubated with shaking at 200 rpm at 30 °C overnight for 20 h. From the mated culture (0.5 mL), 100 μL of 1/10, 1/100 and 1/1000 dilutions were plated on each of the following Petri dishes with agar: SD/–Trp; SD/–Leu; SD/–Leu/–Trp (=DDO); SD/–Leu/–Trp /X-α-Gal/AbA (=DDO/X/A). Cells were grown for 3–5 days at 30 °C.

2.5. Two-Hybrid Library Screening Using Yeast Mating

For library screening, the concentrated bait culture was mixed with 1 mL of the normalized Mate & Plate library (Takara Bio USA, Inc., San Jose, CA, USA) and incubated overnight before plating on DDO/X/A selective medium. A concentrated overnight culture of the Y2HGold-MBP bait strain was prepared. For this, one fresh large (2–3 mm) colony of the bait strain was seeded in 50 mL of SD/–Trp liquid medium. The cells were incubated with shaking (250–270 rpm) at 30 °C until OD_{600} reached 0.8 (20 h). The cells were precipitated by centrifugation (at 1000× *g* for 5 min), after which the supernatant was removed. The pellet was resuspended to a cell density of >1 × 10^8 cells/mL in SD/–Trp liquid media (4–5 mL). Then the library strain was combined with the bait strain. For this, a 1 mL aliquot of the library strain was thawed in a water bath at room temperature. 10 µL was left for titration on 100 mm plates with solid SD/–Leu medium. 1 mL of the Mate & Plate Library was mixed with 4–5 mL of the bait strain in a sterile 2 L flask, and 45 mL of 2× YPDA liquid medium (containing 50 µg/mL of kanamycin) was added. Cells from the library flask were washed twice with 1 mL of 2× YPDA, and washes were added to the 2 L flask. The cells were incubated at 30 °C for 20–24 h with minimal shaking (30–50 rpm). After 20 h, a drop of the culture was checked under a phase contrast microscope (40×) for the presence of zygotes. Since they were present in large numbers, which indicated a successful crossing, the cells were harvested by centrifugation at 1000× *g* for 10 min. The flask was washed twice with 50 mL 0.5× YPDA (with 50 µg/mL kanamycin), the washes were combined and used to resuspend the pelleted cells. The cells were centrifuged at 1000× *g* for 10 min and the supernatant was removed. The pelleted cells were resuspended in 10 mL of 0.5× YPDA/Kan liquid medium. The total volume of the cell suspension was measured. To count the number of clones resulting from the mated culture, 100 µL of 1/10, 1/100, 1/1000 and 1/10,000 dilutions were plated on each of the following 100 mm agar plates and incubated at 30 °C for 3–5 days: SD/–Trp; SD/–Leu; SD/–Leu/–Trp. The rest of the cell culture was plated by adding 100 µL onto 120 100 mm plates with DDO/X/A agar medium. The library was allowed to grow at 30 °C for 3–5 days. All blue colonies that grew on DDO/X/A medium were streaked onto plates with QDO/X/A agar (SD/–Ade/–His/–Leu/–Trp/X-α-Gal/AbA) with a higher stringency using sterile yellow pipette tips.

2.6. Analysis of Positive Interactions by PCR

For primary positive colony screening by PCR, DNA from blue yeast colonies on QDO/X/A was isolated using a DNA-Sorb-AM kit (Federal Budget Institution of Science «Central Research Institute of Epidemiology» of the Federal Service for Surveillance on Consumer Rights Protection and Human Wellbeing, Moscow, Russia) and used as a template in PCR using primers MM_screen_For and MM_screen_Rev, flanking the expressed inserts in pGADT7 plasmid. The primer sequences are 5′-CTATTCGATGATGAAGATACCCCACCA AACC-3′ for MM_screen_For and 5′-GTGAACTTGCGGGGTTTTTCAGTATCTACGATT-3′ for MM_screen_Rev. The PCR conditions were the following: 300 s at 95 °C, 30 cycles of 420 s at 72 °C and 15 s at 95 °C with a final extension of 600 s at 72 °C. PCR products were resolved in 1% agarose gel containing 0.5 µg/mL of ethidium bromide. Positive bands were excised from the gel, purified by QIAquick Gel Extraction Kit (Qiagen, Hilden, Germany), and their nucleotide sequences were determined by Sanger sequencing with T7 Sequencing Primer.

2.7. Confirmation of MBP-Bri23R Positive Interactions in Y2HGold Yeast Strain

Using the small-scale transformation procedure, 100 ng of each of the following pairs of vectors (pGBKT7/MBP + Bri23R in pGADT7; empty pGBKT7 + Bri23R in pGADT7) were cotransformed into Y2HGold competent cells. 100 µL of 1/10 and 1/100 dilutions of the transformation mixes were spread on the DDO/X and QDO/X/A plates. The results of the genuine interaction of MBP with Bri23R were represented by blue colonies grown on DDO/X and QDO/X/A plates for pGBKT7/MBP + Bri23R in pGADT7 pair and white

colonies on DDO/X and no colonies on QDO/X/A plates for the empty pGBKT7 + Bri23R in pGADT7 pair (see Supplementary Figure S1). False positives would give blue colonies on any plate for both pairs.

2.8. Additional Confirmation of MBP-Bri23R Positive Interactions in Y2HGold Yeast Strain Using Reciprocal Approach

MBP and Bri23R coding sequences were reversely cloned in pGADT7 and pGBKT7 plasmids, respectively. For this, the NdeI/XhoI MBP fragment from p.2.1 of Methods above was cloned in pGADT7 digested with NdeI/XhoI, and Bri23R coding fragment was amplified from Bri23R/pGADT7 using MM_screen_For and MM_screen_Rev primers (300 s at 95 °C, 20 cycles of 60 s at 72 °C and 15 s at 95 °C with a final extension of 420 s at 72 °C), digested with NdeI/XhoI and cloned in pGBKT7 digested with NdeI/SalI.

Then the reciprocal analysis for interaction was performed the same as described in p.2.8 of Methods above for direct mode interaction, except the following pairs of plasmids were used: pGBKT7/Bri23R + MBP/pGADT7; pGBKT7/Bri23R + pGADT7. The results were shown in Supplementary Figure S6, where pGBKT7/Bri23R + MBP/pGADT7 plasmid pair gave blue colonies on both DDO/X and QDO/X/A plates, and pGBKT7/Bri23R + pGADT7 plasmid pair gave white colonies and no colonies on DDO/X and QDO/X/A plates, respectively, confirming true MBP-Bri23R interaction (see Supplementary Figure S1).

2.9. AlphaFold2-Based Modeling

AlphaFold2-built models of human Bri2 (UniProt ID Q9Y287) and yeast regulatory protein Gal4 (UniProt ID P04386) were downloaded from the UniProt database (https://www.uniprot.org/, accessed on 10 October 2021). Models of human MBP isoform 5 (UniProt ID P02686-5) and fusion proteins, in which MBP and 24 C-terminal amino acids of Bri2 (Bri23R) were fused at the C-termini of the N- and C-terminal domains of Gal4, respectively, or vice versa, were prepared using AlphaFold2 colab service (https://colab.research.google.com/github/deepmind/alphafold/blob/main/notebooks/AlphaFold.ipynb, accessed on 10 October 2021) [3,4]. The amino acid sequences of the modeled fusion proteins are presented in Supplementary Figure S2. All modeled structures were visualized using PyMOL.

The qualities of the models were validated using the AlphaFold lDDT-Cα metric (Supplementary Figure S3), which produces a chart of per-residue estimated confidence on a scale from 0 to 100. Regions with pLDDT > 90 are expected to have very high confidence, regions with pLDDT between 70 and 90 are expected to have good confidence, regions with pLDDT between 50 and 70 are of low confidence, and pLDDT < 50 is a strong predictor of IDP suggesting that such region is either unstructured in physiological conditions or only structured as part of a complex.

2.10. Docking Calculations

The 3D models of the complexes were obtained with high ambiguity driven protein-protein docking (HADDOCK 2.1) [25,26]. The docking algorithm has three stages. At first, rigid body docking was performed, in which interacting molecules were rotated and translated randomly in turn to minimize intermolecular energy. It was followed by the annealing stage, in which annealing of torsion angle space was performed to refine the orientation of the molecules and the side chains and/or backbones of the interface residues. The last stage was solvent refinement in which the structures were further refined in explicit solvent layers. The 3D coordinates of six AlphaFold2-built models were used in the calculation.

HADDOCK presupposes the use of the defined intermolecular ambiguous interaction constraints (AIR) in the calculations. The AIR residues are assumed to have no less than 40% solvent accessible surface area. Surface accessibilities were assessed with the program FreeSASA [27]. Unless otherwise specified, solvent accessible residues of Bri23R and MBP were suggested as AIR.

The 1000 structures of the complexes were calculated with the rigid docking protocol. The 200 structures with the lowest AIR violations were energy minimized with the side chains left flexible. Then the 30 best structures were minimized again in an 8 Å shell of explicit TIP3P water [28]. These best structures were grouped into clusters based on the FCC clustering algorithm [29]. The buried surface area in the complexes was analyzed and visualized using PyMOL and PDBePisa [30].

3. Results and Discussion

3.1. Interaction of MBP with a C-Terminal Peptide of Bri2 Was Discovered Using a Yeast Two Hybrid System

To identify the spectrum of proteins interacting with MBP, Matchmaker Gold Y2HS was used. In a Matchmaker GAL4-based two-hybrid assay, a bait protein is expressed as a fusion to the Gal4 DNA-binding domain (Gal4BD), while libraries of prey proteins are expressed as fusions to the Gal4 activation domain (Gal4AD) [23]. In the Y2HS, when the bait and library (prey) fusion proteins interact, the Gal4BD and Gal4AD are brought into proximity to activate transcription of four independent reporter genes: *AUR1-C*, *ADE2*, *HIS3*, and *MEL1* (Figure 1A).

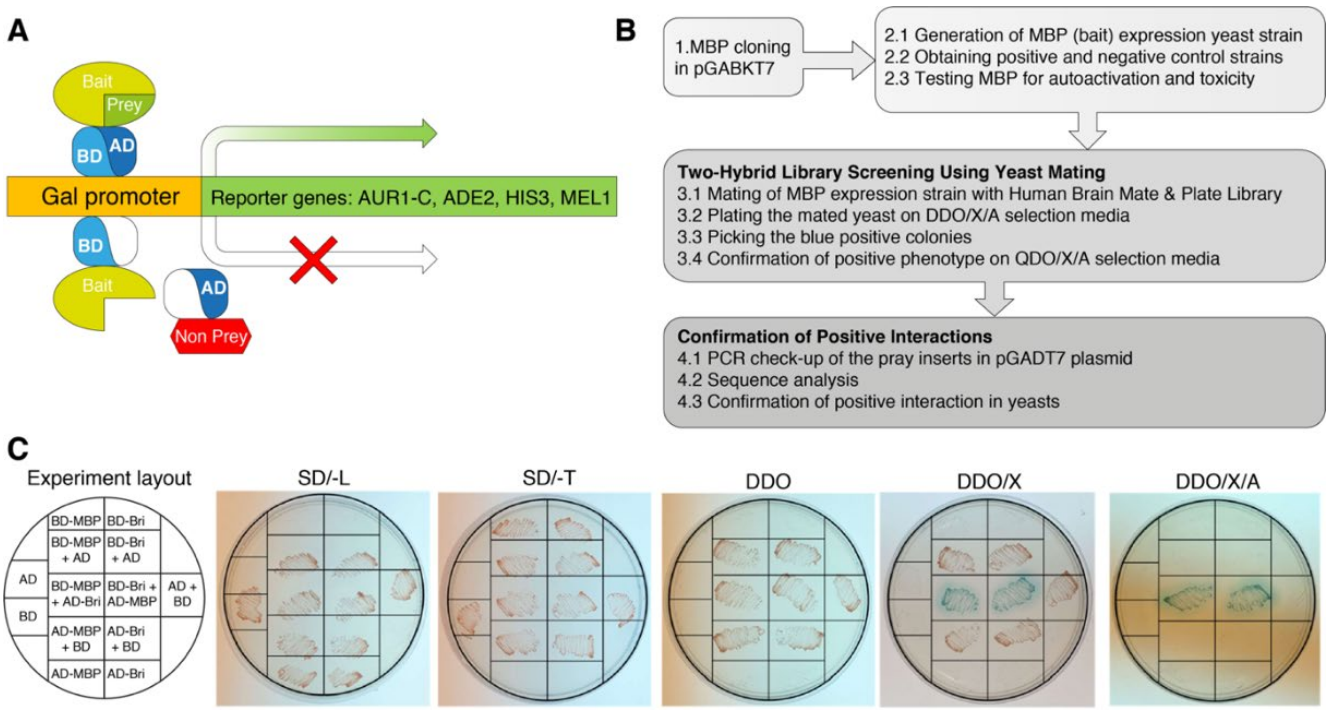

Figure 1. Experiment schematics. (**A**) Principle of a two-hybrid yeast system for the detection of protein-protein interactions. One protein is expressed as a GAL4BD fusion protein, and another protein is expressed as a GAL4AD fusion protein. When they interact, BD and AD are brought into proximity and activate the transcription of the reporter genes *AUR1-C*, *ADE2*, *HIS3*, and *MEL1*, allowing selection. (**B**) Flow chart of procedures for two-hybrid identification of proteins interacting with MBP. (**C**) Validation assay in yeasts to confirm MBP-Bri23R interaction. The transformed clones were streaked on the plates with the selection media. The detailed scheme of the validation assay is provided in Supplementary Figure S1.

In Clontech's *Saccharomyces cerevisiae* Y2H Gold strain, which is used to detect two-hybrid interactions, the aforementioned integrated reporter genes are under the control of three distinct Gal4-responsive promoters. *AUR1-C* is a dominant mutant version of the *AUR1* gene that encodes the enzyme inositol phosphoryl ceramide synthase. The expression of *AUR1-C* confers strong resistance to the otherwise highly toxic drug Aureobasidin A. This drug reporter is preferable to nutritional reporters alone, due to lower background

activity. *HIS3*: Y2HGold is unable to synthesize histidine and is, therefore, unable to grow on media that lacks this essential amino acid. Gal4-responsive *HIS3* expression permits cells to biosynthesize histidine and grow on His-minus minimal medium. *ADE2*: Y2HGold is also unable to grow on minimal media that does not contain adenine. However, when the *Ade2* expression is activated, the cells can grow on minimal medium without adenine. *MEL1* encodes α-galactosidase, an enzyme occurring naturally in many yeast strains, which is expressed and secreted by yeast, and yeast colonies that express Mel1 turn blue in the presence of the chromogenic substrate X-α-Gal.

To produce bait fusion protein Gal4BD-MBP, containing the Gal4BD at its N-terminal end and MBP at its C-terminus, we inserted human MBP coding sequence in the ORF of GAL4BD into the pGBKT7 and generated pGBKT7-MBP (Figure 1B).

Before the screening process, we obtained the Y2HGold strain transformed with the pGBKT7-MBP bait plasmid and performed all the necessary check-ups for the GAL4-MBP fusion potential toxicity and autoactivation properties according to the manufacturer's instructions. To generate positive and negative control strains we used plasmid constructs supplied in the kit (pGBKT7-53 Control vector, which encodes the Gal4BD fused with murine p53; pGADT7-T Control vector, encodes the Gal4AD fused with SV40 large T-antigen; and pGBKT7-Lam Control vector, which encodes the Gal4BD fused with lamin). pGBKT7-53 and pGADT7-T plasmids are used to create a positive control strain, as well as pGBKT7-Lam and pGADT7-T plasmids that are used to create negative control strain.

As prey, we used Takara's Mate & Plate Library—Human Brain (Normalized). This yeast two-hybrid library was constructed from mRNA isolated from human brain tissue and transformed into yeast strain Y187. The cDNA was normalized prior to library construction to reduce the copy number of abundant cDNAs derived from highly represented mRNAs, thereby increasing the representation of low copy number transcripts.

For screening, the obtained yeast strain Y2HGold-MBP was mated with Mate & Plate Library in Y187 strain. Primary interactions between respective proteins were identified by growth on double dropout selective media (QDO/X/A) and blue color development. All primary signals were streaked onto plates with quadruple dropout selective media (QDO/X/A) agar providing higher selection stringency. Colonies growing and maintaining the blue color on QDO/X/A agar were subjected to PCR analysis of the inserts in the pGADT7 plasmid. In total, about 200 primary potentially positive clones were selected for analysis, which number was reduced to 56 in QDO/X/A and finally to the 17 unique clones after removing duplicates by PCR and sequence analysis.

Finally, of the identified 17 unique positive signals, only one clone corresponded to the coding region of the protein (Supplementary Table S1, the coding clone highlighted in bold). This protein was identified as ITM2B/Bri2 (Integral transmembrane protein II associated with familial British and Danish dementia (FBD and FDD)), with Genebank ID NM_021999.5 and Uniprot ID Q9Y287. The found clone encoded C-terminal 24-residue peptide of Bri2 (see Figure 2B for illustration).

Table 1. The description of the fusion proteins, which were used in the computational study.

Name	N-Terminus	C-Terminus
	Domain of Gal4, AA, Color *	**Protein, AA, Color ***
Gal4BD-MBP	N-term., 1–147, light gray	MBP-5, full, salmon/cyan
Gal4AD-Bri23R	C-term., 768–881, dark gray	Bri2, 243–266, magenta/green
Gal4AD-MBP	C-term., 768–881, dark gray	MBP-5, full, salmon/cyan
Gal4BD-Bri23R	N-term., 1–147, light gray	Bri2, 243–266, magenta/green

* color coding in Figure 2 and Supplementary Figure S2.

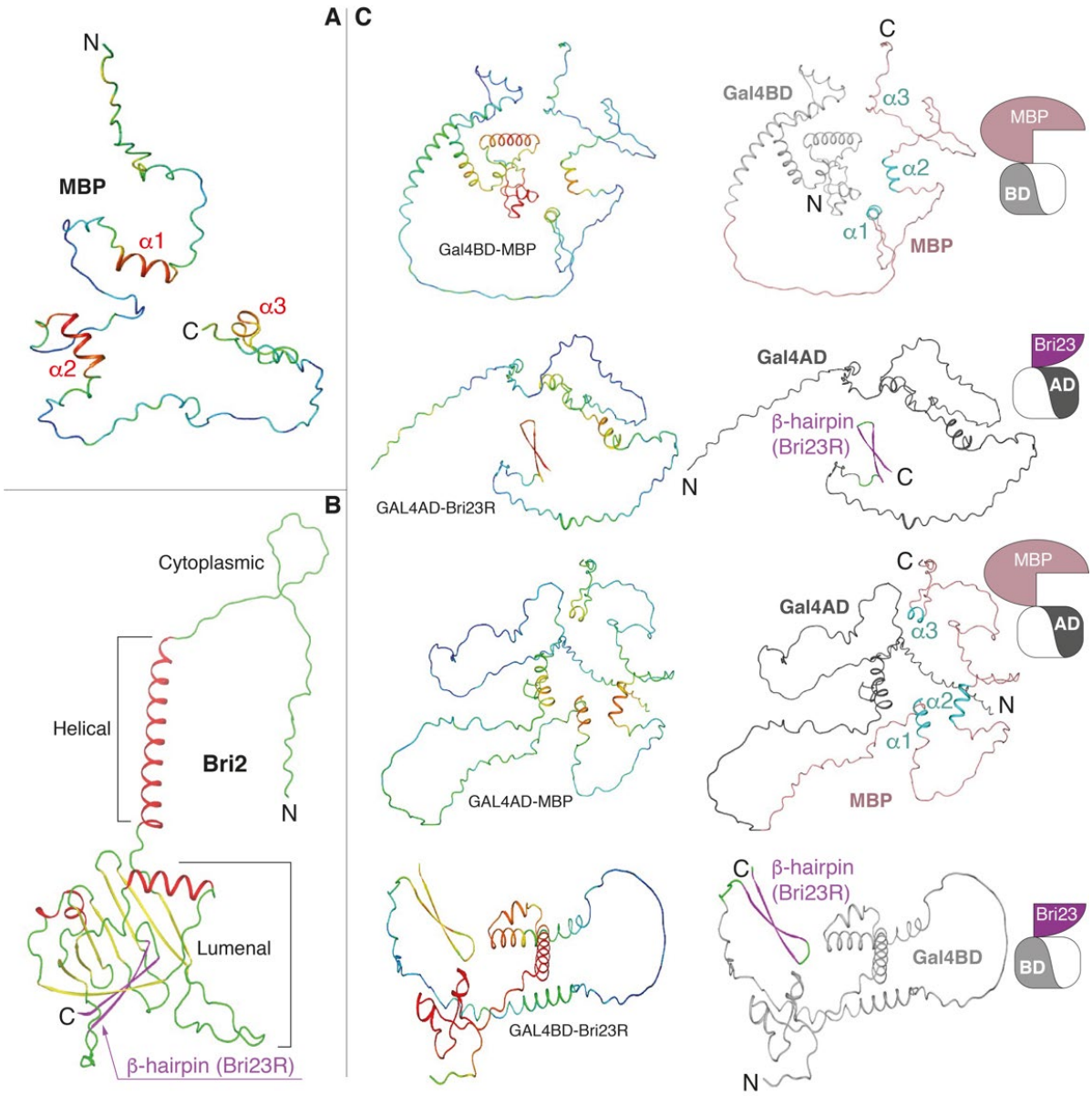

Figure 2. AlphaFold2-built 3D models. (**A**) MBP is colored according to the model confidence level: red—high confidence, blue—low confidence. (**B**) Bri2 is colored according to the secondary structure elements: coils, α-helices and β-strands are in green, red and yellow colors, respectively, with C-terminal β-hairpin (Bri23R) marked by magenta. (**C**) Fusion proteins, in which MBP and Bri23R were fused at the C-termini of Gal4BD and Gal4AD, respectively, or vice versa. Coloring is according to the model confidence (left panels) and domain organization (right panels): Gal4AD—dark gray, Gal4BD—light gray; in MBP, salmon and cyan colors correspond coils and α-helices, respectively; in Bri23R, magenta and green colors correspond β-strands and coils, respectively. See Table 1 and pictograms on the right side for illustration.

Bri2 is a 266 amino acid long transmembrane protein of type 2 consisting of a cytoplasmic domain, helical transmembrane domain and luminal domain [31]. It has a suggested role in neuronal maturation and differentiation [32]. Two different autosomal dominant mutations in the *ITM2B* gene are associated with the aforementioned forms of early-onset dementia [31]. Disease-associated mutations caused the expression of C-terminally extended 277 amino acid long Bri2 proteins, whose furin-dependent proteolysis

generated 34 amino acid long peptides (ABri in FBD and ADan in FDD) that accumulated into neurotoxic amyloid aggregates.

To date, the exact physiological function of Bri2 has not been fully elucidated. However, its interaction with Amyloid precursor protein (APP) and involvement in the regulation of APP processing and inhibition of beta-amyloid production was shown [33]. This function as a modulator of APP processing is associated with Bri2 maturation, which started with furin-dependent cleavage of the C-terminal 23 amino acid long Bri23 peptide from immature Bri2 during its transport in the Golgi [34]. This Bri23 peptide itself prevents the aggregation of APP amyloid-beta protein 42 into toxic oligomers [35]. Truncated Bri2 undergoes further proteolytic processing by ADAM10, which cuts out the extracellular 100 amino acid long evolutionary conserved Brichos domain, and by Signal Peptidase-Like 2B, which cleaves the remaining membrane-bound polypeptide [36].

The 24-residue peptide found by means of the two-hybrid system represents Bri23 peptide with R residue attached at the N-terminus (Bri23R). Interaction between Bri23R and MBP was confirmed in yeasts on selective media using the yeast cotransformation procedure in direct and reciprocal modes where protein-coding inserts were switched between the plasmids coding for Gal4BD and -AD domains (procedure details are described in pp.2.7 and 2.8 of Methods, and results are presented in Figure 1C and Supplementary Figure S1). It should be noted, that in 2018, Rebelo's group conducted a study of the Bri2 interactome in the brain [37]. MBP was identified among the proteins co-precipitated with Bri2 from brain tissue. However, further studies on the specificity of their interaction have not been carried out. These data raised the question what form or domain of Bri2 is actually involved in the interaction with MBP.

3.2. Molecular Modeling and Characterization of the Putative Complexes between MBP and the C-Terminal β-Hairpin of Bri2

The 3D models of human MBP and Bri23R as well as those of four fusion proteins, described in Table 1, were prepared by means of AlphaFold2. The sequences of the fusion proteins were identical to those of the interacting protein components in the yeast two-hybrid system (Supplementary Figure S2).

All obtained 3D models are shown in Figure 2 with the confidence (pLDDT) level color-mapped in the 3D structures. As stated earlier, MBP is an intrinsic disordered protein (IDP), although three α-helices (α1, α2 and α3), predicted with the confidence level from good to high, were clearly visible in the structures (Figure 2A,C and Supplementary Figure S3). The 24 C-terminal amino acids of Bri2 (Bri23R—the Bri23 peptide [36] with one additional R residue at the N-terminus) always form a stable β-hairpin predicted with good confidence (Figure 2B,C and Supplementary Figure S3). In the case of the luminal domain of native Bri2, this β-hairpin participates in the formation of a curved β-sheet (Figure 2B), in which it is partially buried; but, as we explained above, the Bri23 peptide is cleaved from Bri2 during its maturation in the Golgi [34,35]. Both Gal4 domains contain α-helical and disordered areas. The α-helical core of Gal4BD is predicted with high accuracy, while Gal4AD is mostly disordered with a small α-helical region predicted with moderate accuracy (Figure 2C and Supplementary Figure S3). Superimposition at the Cα-atoms of MBP and Gal4 domains from the fusion proteins with those in their native prototypes showed that the secondary structure composition and general structural topologies were similar (data not shown).

Using a data-driven docking program HADDOCK, three types of complexes were designed: Gal4BD-MBP/Gal4AD-Bri23R, Gal4AD-MBP/Gal4BD-Bri23R and MBP/Bri23R (a complex of MBP with the 24 C-terminal amino acid of Bri2). The first two complexes correspond to two variants of the fusion proteins, whose interactions were detected by the Y2HS (see Supplementary Figure S1), while in the third complex neither MBP nor Bri23R was fused to the Gal4 domains and thus, represented native proteins actually existing in cells of higher eukaryotes.

The characteristics of the best clusters generated from the 30 final complexes in all three cases are summarized in Table 2. The lowest energy structures representing the

obtained clusters are shown in Figure 3 for the Gal4BD-MBP/Gal4AD-Bri23R and Gal4AD-MBP/Gal4BD-Bri23R complexes and in Figure 4 for the MBP/Bri23R complex.

Table 2. Statistical analysis of the lowest energy clusters obtained for the best 30 HADDOCK-generated complexes.

N.	Size #	RMSD [1], Å	Intermolecular Energy, kcal/mol Average/SD				Buried Surface Area [2], Å	HADDOCK Score [2]
			Total	Vdw [3]	Elec [3]	AIR [3]		
Gal4BD-MBP/Gal4AD-Bri23R								
1	11	2.2/0.8	−313.8/56.1	−54.6/8.5	−259.2/55.8	505.6/86.7	2195.2/202.5	−57.3/14.2
2	9	1.5/0.6	−360.1/43.2	−39.1/10.4	−321.0/37.1	439.5/54	2044.9/205.0	−48.4/16.0
3	5	2.9/1.6	−354.3/68.2	−82.4/16.7	−271.9/55.8	430.5/69.5	3035.8/345.4	−120.4/39.8
Gal4AD-MBP/Gal4BD-Bri23R								
1	5	2.5/1.3	−307.4/52.6	−53.7/10.8	−253.7/56.1	476.8/53.7	2149.4/175.3	−97.3/13.2
2	4	1.2/0.8	−152.9/10.0	−42.6/13.4	−110.3/3.6	361.0/28.6	2060.1/188.5	−62.6/17.9
3	4	3.3/1.9	−185.6/20.9	−33.9/3.9	−151.7/20.7	534.0/99.1	2005.5/148.3	−58.5/19.5
MBP/Bri23R [4]								
16	5	1.4/0.7	−254.4/35.9	−36.7/2.8	−217.7/37.7	3643.4/255.0	1750.4/140.0	288.2/17.9
18	4	1.5/09	−215.0/10.2	−40.6/6.8	−174.4/4.0	3688.6/100.5	1952.9/101.8	268.4/9.2
MBP/Bri23R [4] (docking with residues from the α-helices chosen as AIR)								
19	7	1.1/05	−128.0/31.5	−40.6/3.9	−87.5/31.0	280.9/80.4	1519.7/94.5	−70.2/9.8
30	9	1.7/0.8	−126.2/28.5	−21.2/10.3	−105.0/32.0	273.9/35.1	1514.3/57.4	−54.7/9.5

the number of models in the cluster. [1] Average and standard deviation were calculated by comparing with the lowest energy structure from the same cluster. [2] Average value and standard deviation for all structures from the same cluster. [3] Van der Waals (Vdw), electrostatic (Elec), and AIR energy for the intermolecular interaction calculated with HADDOCK. [4] Numbering of clusters is according to the automatic enumeration of their representative structures generated by HADDOCK.

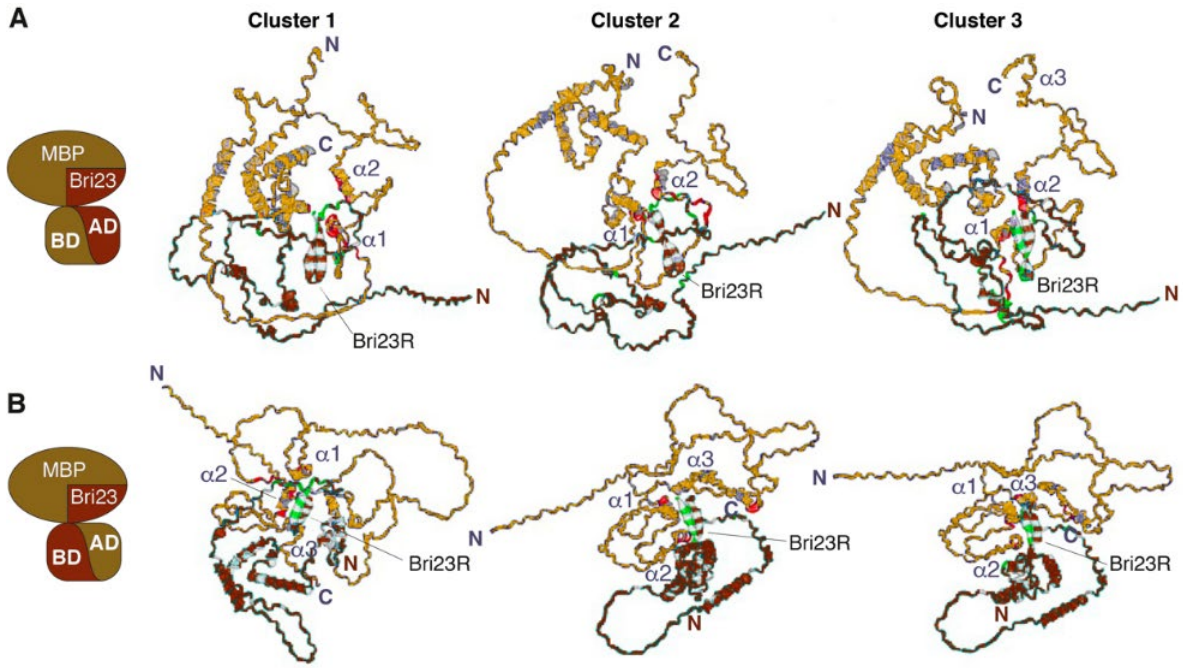

Figure 3. HADDOCK-predicted complexes Gal4BD-MBP/Gal4AD-Bri23R (**A**) and Gal4AD-MBP/Gal4BD-Bri23R (**B**). The representative structures of lowest energy clusters (see Table 2 for description) obtained for the best 30 HADDOCK-generated complexes are shown as ribbon-mesh pictograms generated by PDBePISA. MBP-containing fusion proteins are colored gold, while Bri23R-containing fusion proteins are colored brown (see pictograms at the left for illustration); the main chains of interacting residues from the binding interfaces are marked by red and green color, respectively.

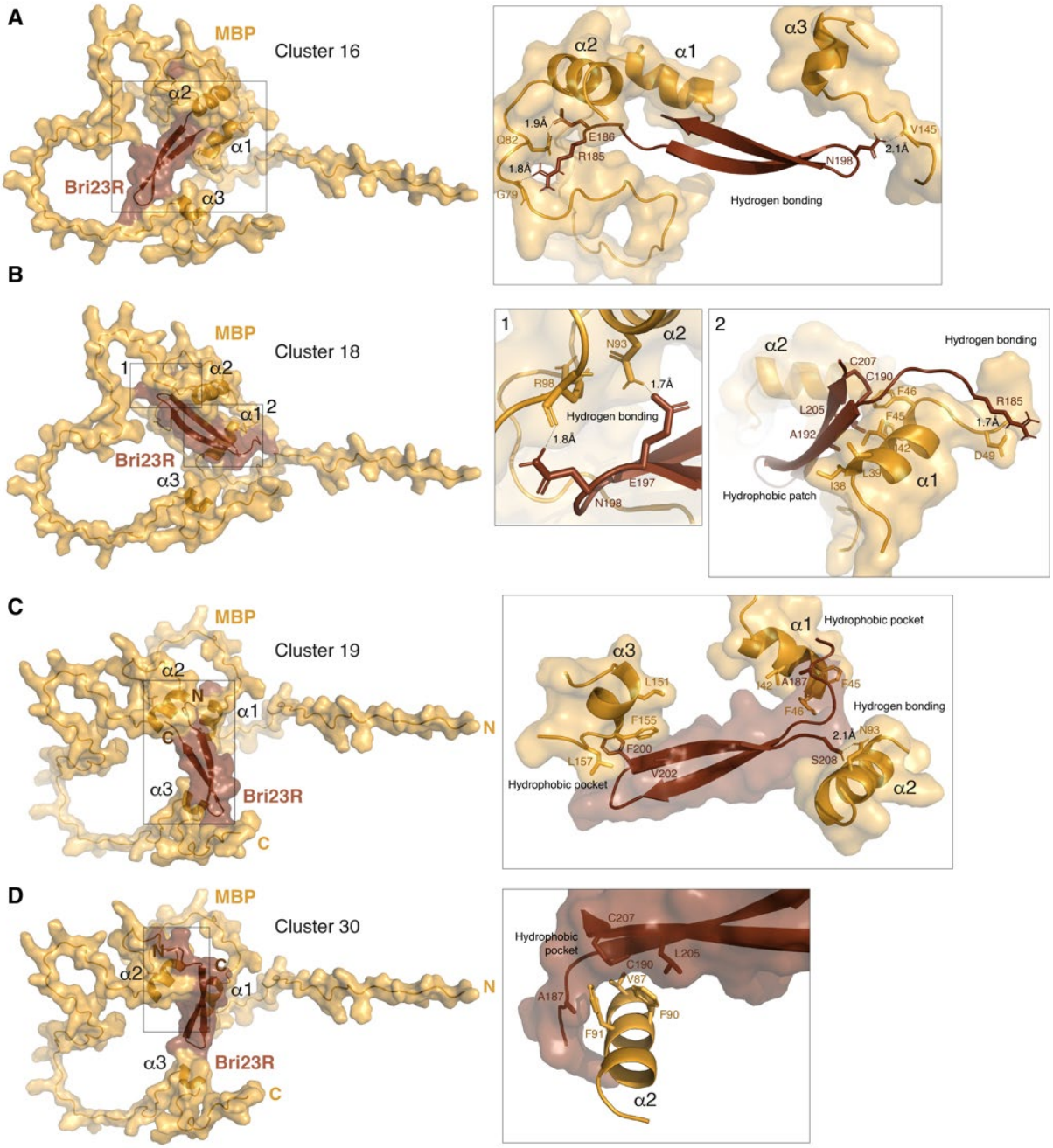

Figure 4. HADDOCK-predicted complexes MBP/Bri23R. The representative structures of lowest energy clusters obtained for the best 30 HADDOCK-generated complexes are shown as surface/ribbon pictograms generated by PyMol and numbered 16 (**A**), 18 (**B**), 19 (**C**) and 30 (**D**) according to their automatic enumeration generated by HADDOCK. MBP is colored bright orange and Bri23R is colored chocolate. Details of polar and hydrophobic intermolecular interactions are shown in the inserts on the right side. Interacting residues are shown by sticks.

Three main clusters were identified from the 30 lowest-energy structures generated for either the Gal4BD-MBP/Gal4AD-Bri23R or Gal4AD-MBP/Gal4BD-Bri23R complex (Table 2). The average intermolecular energies of these clusters were higher in the first complex (from 360.1 to 313.8 kcal/mol) compared to those in the second complex (from 307.4 to 152.9 kcal/mol). However, the best models for the Gal4AD-MBP/Gal4BD-Bri23R complex were compatible with those for the Gal4BD-MBP/Gal4AD-Bri23R complex, while two other less energy-efficient clusters were similar to each other (Figure 3B). The major

contribution in the intermolecular energies was from the electrostatic component, which indicates a significant impact of polar interactions in the formation of the complexes.

Residues involved in the putative binding interfaces and intermolecular contacts between them were evaluated using PDBePISA. The analysis of the intermolecular salt bridges and hydrogen bonds in the representative structures of the best clusters for the Gal4BD-MBP/Gal4AD-Bri23R and Gal4AD-MBP/Gal4BD-Bri23R complexes are shown in Supplementary Tables S2 and S3, respectively. The binding interfaces and residues participating in either polar or hydrophobic contacts are marked in Figure 3 and color-mapped in the sequences of the interacting proteins in Supplementary Figures S4 and S5, respectively. In accordance with enhanced intermolecular energies, a higher number of interfacial residues involved in the intermolecular polar contacts were detected in the best models of the Gal4BD-MBP/Gal4AD-Bri23R complex compared to those of the Gal4AD-MBP/Gal4BD-Bri23R complex (Supplementary Tables S2 and S3). These residues formed from six to twelve polar contacts between the Gal4BD-MBP and Gal4AD-Bri23R molecules, the majority of which were between MBP and Bri23R components of the fusion proteins (Supplementary Table S2). Two to four polar contacts were found in the representative structures of the Gal4AD-MBP/Gal4BD-Bri23R complex (Supplementary Table S3). At the same time, the Van der Waals energy of the intermolecular interactions was similar for both Gal4BD-MBP/Gal4AD-Bri23R and Gal4AD-MBP/Gal4BD-Bri23R complexes (Table 2).

The location of the interacting residues in the binding interfaces varied between different clusters of each complex, though the residues from Bri23R and at least two α-helices (α1 and α2) of MBP, as well as their nearest surroundings, were always involved (Figure 3, Supplementary Figures S4 and S5). In addition to the intermolecular contacts between MBP and Bri23R, other components of the fusion proteins including Gal4AD, Gal4BD and connecting linkers were involved in the complex formation, which was in accordance with activation of the Gal4-induced metabolic pathways in the yeast cells expressing complementing pairs of fusion proteins: either Gal4BD-MBP and Gal4AD-Bri23R or Gal4AD-MBP and Gal4BD-Bri23R (Supplementary Tables S2 and S3).

As we mentioned above, in addition to the evaluation of the putative complexes between MBP- and Bri23R-containing fusion proteins interacting in the Y2HS, the same approach, in which AlphaFold2-based modeling was complemented with HADDOCK-based docking and PDBePISA-based structural analysis was applied to evaluate a suggested interaction between MBP and Bri23R in their native forms. Since the predominant participation of the two α-helices of MBP in the interaction with Bri23R was detected during docking of the fusion proteins; the modeling of the MBP/Bri23R complex was carried out in two variants, specifying either the entire solvent accessible surface of MBP as AIR or only amino acid residues from the alpha-helices. Two main clusters were identified among the 30 lowest-energy structures in either calculation (Table 2 and Figure 4). More energy-efficient clusters were obtained in the first case; the major contribution in the increasing intermolecular energies was from the electrostatic component, which was associated with an enhanced amount of the interfacial polar contacts (Supplementary Table S4 and Figure S6). All four clusters were less energy-efficient than either the Gal4BD-MBP/Gal4AD-Bri23R complexes or the best cluster of the Gal4AD-MBP/Gal4BD-Bri23R complex; however, the binding energies were compatible with or prevailed over those of two less energy-efficient clusters of the Gal4AD-MBP/Gal4BD-Bri23R complex. Given the small size of the Bri23R surface available for intermolecular interactions, such binding energies were rather satisfactory. Moreover, PDBePISA-based analysis showed that cluster # 30 has not only the highest solvation free energy gain from the hydrophobic interactions but the lowest *p*-value, indicating that the suggested interface is supposed to be interaction-specific (Supplementary Table S4).

The analysis of a pattern of the binding interfaces in the MBP surface revealed that similar to the fusion proteins and independently of using or not using the α-helical part of MBP as AIR, at least two α-helices of MBP are predominantly involved in the intermolecular interaction (Figure 4 and Supplementary Figure S6). Further analysis of the four clusters generated for the MBP/Bri23R complex shows that in Bri23R, both free termini of the β-

hairpin and the loop connecting the two β-strands are solvent accessible and involved in the intermolecular interactions (Figure 4 and Supplementary Figure S6). Moreover, according to Figure 4, the interaction with Bri23R causes some structural ordering of MBP, which twists around the β-hairpin so that the size of the internal space between the α-helices is adjusted to the size of the β-hairpin.

Thus, the computational approach, which included AlphaFold2-based modeling and HADDOCK-based docking complemented the results obtained in the yeast two-hybrid system and allowed not only to assume the formation of a complex between MBP and the C-terminal β-hairpin of Bri2, but also the predominant participation of the alpha-helical regions of MBP in the interaction.

It should be noted that β-hairpins are widespread in the protein kingdom and are involved in many protein-protein interactions. This motif is also popular in synthetically designed proteins and peptides due to its stability and adaptability to broad functions [38]. The twisted shape, open edges for hydrogen bonding, and the hydrophobic surfaces of β-hairpin structures provide a unique ability to fold in a variety of ways. However, the relationship between the sequence of β-hairpins and the way they are assembled is far from understood [39]. β-hairpins are attracting great attention as a regulator of amyloidogenesis, which either plays a role in amyloid assembly as key building blocks of amyloid fibrils or preventing the formation of toxic oligomers [40]. It should also be noted that the Simons group has previously shown that MBP forms a barrier in the cytoplasmic space that allows size selection of proteins, thus preventing the diffusion of most soluble and membrane proteins into the myelin sheath [41]. They also showed that the binding of MBP to the inner membrane mediates the formation of a dense protein network, which is similar to the network formed by amyloid fibrils. These amyloid-like interactions provide the molecular basis for protein extrusion and myelin membrane zipping [42]. We suggested that amyloid-like structures associated with MBP accumulation in the inner leaflet of the membrane bilayer can serve as a seed that attracts native Bri23 peptide and initiates its interaction with MBP. Thus, the prevalence and physiological significance of the observed interaction between MBP and the C-terminal β-hairpin of Bri2 should be carefully studied in vivo and in vitro.

4. Conclusions

Two subjects of this study, myelin basic protein (MBP) and integral transmembrane protein II associated with familial British and Danish dementia (ITM2B/Bri2 or Bri2), are involved in neuronal development and degeneration. However, the disordered structure of MBP and the multistep complex proteolytic processing of Bri2 complicate their study and, as a result, the exact physiological and pathological roles of these proteins are far from understood. Here, the interaction of MBP with the C-terminal peptide of Bri2 was discovered using a yeast two-hybrid system that allows the interaction of proteins in their natural environment to be detected. The discovered peptide (Bri23R) mimicked the native one that appeared during Bri2 maturation and had physiological activity as a modulator of amyloid precursor protein processing. In this regard, computational methods of structural biology, including the artificial intelligence system AlphaFold2 and high ambiguity driven protein-protein docking (HADDOCK), were used to obtain a mechanistic explanation of the detected protein-protein interaction and to elucidate the possible structure of the MBP complex with the Rri23R peptide. As expected, MBP was mostly unstructured, although it has well-defined α-helical regions, while Bri23R forms a stable β-hairpin. Simulation of the interaction between MBP and Bri23R showed that MBP twists around the peptide, while the internal space between MBP α-helices is adjusted to the size of the β-hairpin. It is known that β-hairpins are ubiquitous protein structural motives found in molecules throughout the tree of life, which can serve as either inductors or inhibitors of amyloidogenesis. In this regard, since the association of MBP to the inner leaflet of the membrane bilayer shares features with amyloid fibril formation and native Bri23 is known to inhibit amyloid

aggregation, the found MBP-Bri23R interaction indicates that Bri23 may serve as a peptide chaperon for MBP, thus participating in myelin membrane assembly.

Supplementary Materials: The following are available online at https://www.mdpi.com/article/10.3390/cryst12020197/s1, Figure S1. Validation assay in yeasts to confirm MBP-Bri interaction. Figure S2. The names and sequences of the fusion proteins, whose 3D models were used in the study. Figure S3. Quality evaluation of the AlphaFold2-built 3D models of the fusion proteins presented as a per-residue confidence score (pLDDT). Figure S4. Sequences of the fusion proteins with color mapping of binding interfaces on the representative structures of the lowest energy clusters were obtained for the best 30 HADDOCK-generated Gal4BD-MBP/Gal4AD-Bri23R complexes. Figure S5. Sequences of the fusion proteins with color mapping of binding interfaces on the representative structures of the lowest energy clusters were obtained for the best 30 HADDOCK-generated Gal4AD-MBP/Gal4BD-Bri23R complexes. Figure S6. Sequences of MBP and Bri23R with color mapping of binding interfaces on the representative structures of the lowest energy clusters were obtained for the best 30 HADDOCK-generated MBP/Bri23R complexes. Table S1. Unique clones were identified by means of a two-hybrid yeast system. Table S2. Polar interactions in the intermolecular interfaces of the representative structures of the lowest energy clusters were obtained for the best 30 HADDOCK-generated Gal4BD-MBP/Gal4AD-Bri23R complexes. Table S3. Polar interactions in the intermolecular interfaces of the representative structures of the lowest energy clusters were obtained for the best 30 HADDOCK-generated Gal4AD-MBP/Gal4BD-Bri23R complexes. Table S4. The solvation free energy and polar interactions of the intermolecular interfaces of the representative structures of the lowest energy clusters were obtained for the best 30 HADDOCK-generated MBP/Bri23R complexes. Supplementary archive. PDB files of HADDOCK-created models.

Author Contributions: Conceptualization, E.V.S., T.V.R. and A.A.B.J.; methodology, E.V.S. and T.V.R.; software, T.V.R.; validation, E.V.S., T.V.R. and A.A.B.J.; formal analysis, A.A.B.J.; investigation, E.V.S. and T.V.R., G.A.S. and A.A.K.; resources, A.A.B.J. and A.A.K.; data curation, E.V.S. and T.V.R.; writing—original draft preparation, E.V.S. and T.V.R.; writing—review and editing, T.V.R., E.V.S. and A.A.B.J.; visualization, A.A.B.J., E.V.S. and T.V.R.; supervision, A.A.B.J.; project administration, E.V.S.; funding acquisition, A.A.B.J. All authors have read and agreed to the published version of the manuscript.

Funding: This research was funded by the Ministry of Science and Higher Education of the Russian Federation (grant agreement no. 075-15-2020-795, state contract no. 13.1902.21.0027 of 29.09.2020 unique project ID: RF-190220X0027).

Data Availability Statement: All data can be found online at Supplementary Materials. PDB files of HADDOCK-created models.

Acknowledgments: We thank the Center for collective use "Bioorganika" of Shemyakin-Ovchinnikov Institute of Bioorganic Chemistry RAS.

Conflicts of Interest: The authors declare no conflict of interest.

References

1. Senior, A.W.; Evans, R.; Jumper, J.; Kirkpatrick, J.; Sifre, L.; Green, T.; Qin, C.; Žídek, A.; Nelson, A.W.R.; Bridgland, A.; et al. Protein Structure Prediction Using Multiple Deep Neural Networks in the 13th Critical Assessment of Protein Structure Prediction (CASP13). *Proteins Struct. Funct. Bioinform.* **2019**, *87*, 1141–1148. [CrossRef] [PubMed]
2. Senior, A.W.; Evans, R.; Jumper, J.; Kirkpatrick, J.; Sifre, L.; Green, T.; Qin, C.; Žídek, A.; Nelson, A.W.R.; Bridgland, A.; et al. Improved Protein Structure Prediction Using Potentials from Deep Learning. *Nature* **2020**, *577*, 706–710. [CrossRef] [PubMed]
3. Jumper, J.; Evans, R.; Pritzel, A.; Green, T.; Figurnov, M.; Ronneberger, O.; Tunyasuvunakool, K.; Bates, R.; Žídek, A.; Potapenko, A.; et al. Highly Accurate Protein Structure Prediction with AlphaFold. *Nature* **2021**, *596*, 583–589. [CrossRef]
4. Varadi, M.; Anyango, S.; Deshpande, M.; Nair, S.; Natassia, C.; Yordanova, G.; Yuan, D.; Stroe, O.; Wood, G.; Laydon, A.; et al. AlphaFold Protein Structure Database: Massively Expanding the Structural Coverage of Protein-Sequence Space with High-Accuracy Models. *Nucleic Acids Res.* **2021**, *50*, D439–D444. [CrossRef] [PubMed]
5. Niu, Z.; Zhong, G.; Yu, H. A Review on the Attention Mechanism of Deep Learning. *Neurocomputing* **2021**, *452*, 48–62. [CrossRef]
6. LeCun, Y.; Bengio, Y.; Hinton, G. Deep Learning. *Nature* **2015**, *521*, 436–444. [CrossRef]
7. Zweckstetter, M. NMR Hawk-Eyed View of AlphaFold2 Structures. *Protein Sci. Publ. Protein Soc.* **2021**, *30*, 2333–2337. [CrossRef]
8. Higgins, M.K. Can We AlphaFold Our Way Out of the Next Pandemic? *J. Mol. Biol.* **2021**, *433*, 167093. [CrossRef]

9. Tong, A.B.; Burch, J.D.; McKay, D.; Bustamante, C.; Crackower, M.A.; Wu, H. Could AlphaFold Revolutionize Chemical Therapeutics? *Nat. Struct. Mol. Biol.* **2021**, *28*, 771–772. [CrossRef]
10. Ruff, K.M.; Pappu, R.V. AlphaFold and Implications for Intrinsically Disordered Proteins. *J. Mol. Biol.* **2021**, *433*, 167208. [CrossRef]
11. Sorg, B.A.; Smith, M.M.; Campagnoni, A.T. Developmental Expression of the Myelin Proteolipid Protein and Basic Protein MRNAs in Normal and Dysmyelinating Mutant Mice. *J. Neurochem.* **1987**, *49*, 1146–1154. [CrossRef] [PubMed]
12. Campagnoni, A.T.; Campagnoni, C.W. Myelin Basic Protein Gene. In *Myelin Biology and Disorders*; Elsevier: Amsterdam, The Netherlands, 2004; pp. 387–400.
13. Bagheri, H.; Friedman, H.; Siminovitch, K.A.; Peterson, A.C. Transcriptional Regulators of the Golli/Myelin Basic Protein Locus Integrate Additive and Stealth Activities. *PLOS Genet.* **2020**, *16*, e1008752. [CrossRef] [PubMed]
14. Farhadi, H.F.; Lepage, P.; Forghani, R.; Friedman, H.C.H.; Orfali, W.; Jasmin, L.; Miller, W.; Hudson, T.J.; Peterson, A.C. A Combinatorial Network of Evolutionarily Conserved *Myelin Basic Protein* Regulatory Sequences Confers Distinct Glial-Specific Phenotypes. *J. Neurosci.* **2003**, *23*, 10214–10223. [CrossRef] [PubMed]
15. Tamura, T.; Sumita, K.; Hirose, S.; Mikoshiba, K. Core Promoter of the Mouse Myelin Basic Protein Gene Governs Brain-Specific Transcription in Vitro. *EMBO J.* **1990**, *9*, 3101–3108. [CrossRef]
16. Boggs, J.M.; Yip, P.M.; Rangaraj, G.; Jo, E. Effect of Posttranslational Modifications to Myelin Basic Protein on Its Ability to Aggregate Acidic Lipid Vesicles. *Biochemistry* **1997**, *36*, 5065–5071. [CrossRef]
17. Boggs, J.M.; Rangaraj, G. Interaction of Lipid-Bound Myelin Basic Protein with Actin Filaments and Calmodulin. *Biochemistry* **2000**, *39*, 7799–7806. [CrossRef]
18. Bamm, V.V.; De Avila, M.; Smith, G.S.T.; Ahmed, M.A.M.; Harauz, G. Structured Functional Domains of Myelin Basic Protein: Cross Talk between Actin Polymerization and Ca2+-Dependent Calmodulin Interaction. *Biophys. J.* **2011**, *101*, 1248–1256. [CrossRef]
19. Boggs, J.M.; Homchaudhuri, L.; Ranagaraj, G.; Liu, Y.; Smith, G.S.; Harauz, G. Interaction of Myelin Basic Protein with Cytoskeletal and Signaling Proteins in Cultured Primary Oligodendrocytes and N19 Oligodendroglial Cells. *BMC Res. Notes* **2014**, *7*, 387. [CrossRef]
20. De Avila, M.; Vassall, K.A.; Smith, G.S.T.; Bamm, V.V.; Harauz, G. The Proline-Rich Region of 18.5 KDa Myelin Basic Protein Binds to the SH3-Domain of Fyn Tyrosine Kinase with the Aid of an Upstream Segment to Form a Dynamic Complex in Vitro. *Biosci. Rep.* **2014**, *34*, e00157. [CrossRef]
21. Smirnova, E.V.; Rakitina, T.V.; Ziganshin, R.H.; Arapidi, G.P.; Saratov, G.A.; Kudriaeva, A.A.; Belogurov, A.A. Comprehensive Atlas of the Myelin Basic Protein Interaction Landscape. *Biomolecules* **2021**, *11*, 1628. [CrossRef]
22. Harauz, G.; Libich, D. The Classic Basic Protein of Myelin—Conserved Structural Motifs and the Dynamic Molecular Barcode Involved in Membrane Adhesion and Protein-Protein Interactions. *Curr. Protein Pept. Sci.* **2009**, *10*, 196–215. [CrossRef] [PubMed]
23. Fields, S.; Song, O. A Novel Genetic System to Detect Protein–Protein Interactions. *Nature* **1989**, *340*, 245–246. [CrossRef] [PubMed]
24. Chien, C.T.; Bartel, P.L.; Sternglanz, R.; Fields, S. The Two-Hybrid System: A Method to Identify and Clone Genes for Proteins That Interact with a Protein of Interest. *Proc. Natl. Acad. Sci. USA* **1991**, *88*, 9578–9582. [CrossRef] [PubMed]
25. Dominguez, C.; Boelens, R.; Bonvin, A.M.J.J. HADDOCK: A Protein−Protein Docking Approach Based on Biochemical or Biophysical Information. *J. Am. Chem. Soc.* **2003**, *125*, 1731–1737. [CrossRef] [PubMed]
26. de Vries, S.J.; van Dijk, A.D.J.; Krzeminski, M.; van Dijk, M.; Thureau, A.; Hsu, V.; Wassenaar, T.; Bonvin, A.M.J.J. HADDOCK versus HADDOCK: New Features and Performance of HADDOCK2.0 on the CAPRI Targets. *Proteins* **2007**, *69*, 726–733. [CrossRef] [PubMed]
27. Mitternacht, S. FreeSASA: An Open Source C Library for Solvent Accessible Surface Area Calculations. *F1000Research* **2016**, *5*, 189. [CrossRef] [PubMed]
28. Jorgensen, W.L.; Chandrasekhar, J.; Madura, J.D.; Impey, R.W.; Klein, M.L. Comparison of Simple Potential Functions for Simulating Liquid Water. *J. Chem. Phys.* **1983**, *79*, 926–935. [CrossRef]
29. Rodrigues, J.P.G.L.M.; Trellet, M.; Schmitz, C.; Kastritis, P.; Karaca, E.; Melquiond, A.S.J.; Bonvin, A.M.J.J. Clustering Biomolecular Complexes by Residue Contacts Similarity. *Proteins Struct. Funct. Bioinform.* **2012**, *80*, 1810–1817. [CrossRef]
30. Krissinel, E.; Henrick, K. Inference of Macromolecular Assemblies from Crystalline State. *J. Mol. Biol.* **2007**, *372*, 774–797. [CrossRef]
31. Tsachaki, M.; Ghiso, J.; Efthimiopoulos, S. BRI2 as a Central Protein Involved in Neurodegeneration. *Biotechnol. J.* **2008**, *3*, 1548–1554. [CrossRef]
32. Martins, F.; Serrano, J.B.; Müller, T.; da Cruz e Silva, O.A.B.; Rebelo, S. BRI2 Processing and Its Neuritogenic Role Are Modulated by Protein Phosphatase 1 Complexing: BRI2:PP1 C OMPLEX F UNCTION IN N EURITOGENESIS. *J. Cell. Biochem.* **2017**, *118*, 2752–2763. [CrossRef]
33. Fotinopoulou, A.; Tsachaki, M.; Vlavaki, M.; Poulopoulos, A.; Rostagno, A.; Frangione, B.; Ghiso, J.; Efthimiopoulos, S. BRI2 Interacts with Amyloid Precursor Protein (APP) and Regulates Amyloid β (Aβ) Production. *J. Biol. Chem.* **2005**, *280*, 30768–30772. [CrossRef] [PubMed]
34. Matsuda, S.; Matsuda, Y.; Snapp, E.L.; D'Adamio, L. Maturation of BRI2 Generates a Specific Inhibitor That Reduces APP Processing at the Plasma Membrane and in Endocytic Vesicles. *Neurobiol. Aging* **2011**, *32*, 1400–1408. [CrossRef] [PubMed]

35. Kim, J.; Miller, V.M.; Levites, Y.; West, K.J.; Zwizinski, C.W.; Moore, B.D.; Troendle, F.J.; Bann, M.; Verbeeck, C.; Price, R.W.; et al. BRI2 (ITM2b) Inhibits A Deposition In Vivo. *J. Neurosci.* **2008**, *28*, 6030–6036. [CrossRef] [PubMed]
36. Martin, L.; Fluhrer, R.; Reiss, K.; Kremmer, E.; Saftig, P.; Haass, C. Regulated Intramembrane Proteolysis of Bri2 (Itm2b) by ADAM10 and SPPL2a/SPPL2b. *J. Biol. Chem.* **2008**, *283*, 1644–1652. [CrossRef]
37. Martins, F.; Marafona, A.M.; Pereira, C.D.; Müller, T.; Loosse, C.; Kolbe, K.; da Cruz e Silva, O.A.B.; Rebelo, S. Identification and Characterization of the BRI2 Interactome in the Brain. *Sci. Rep.* **2018**, *8*, 3548. [CrossRef] [PubMed]
38. DuPai, C.D.; Davies, B.W.; Wilke, C.O. A Systematic Analysis of the Beta Hairpin Motif in the Protein Data Bank. *Protein Sci.* **2021**, *30*, 613–623. [CrossRef]
39. Salveson, P.J.; Spencer, R.K.; Kreutzer, A.G.; Nowick, J.S. X-Ray Crystallographic Structure of a Compact Dodecamer from a Peptide Derived from Aβ $_{16–36}$. *Org. Lett.* **2017**, *19*, 3462–3465. [CrossRef]
40. Hoyer, W.; Grönwall, C.; Jonsson, A.; Ståhl, S.; Härd, T. Stabilization of a Beta-Hairpin in Monomeric Alzheimer's Amyloid-Beta Peptide Inhibits Amyloid Formation. *Proc. Natl. Acad. Sci. USA* **2008**, *105*, 5099–5104. [CrossRef]
41. Aggarwal, S.; Yurlova, L.; Snaidero, N.; Reetz, C.; Frey, S.; Zimmermann, J.; Pähler, G.; Janshoff, A.; Friedrichs, J.; Müller, D.J.; et al. A Size Barrier Limits Protein Diffusion at the Cell Surface to Generate Lipid-Rich Myelin-Membrane Sheets. *Dev. Cell* **2011**, *21*, 445–456. [CrossRef]
42. Aggarwal, S.; Snaidero, N.; Pähler, G.; Frey, S.; Sánchez, P.; Zweckstetter, M.; Janshoff, A.; Schneider, A.; Weil, M.-T.; Schaap, I.A.T.; et al. Myelin Membrane Assembly Is Driven by a Phase Transition of Myelin Basic Proteins Into a Cohesive Protein Meshwork. *PLoS Biol.* **2013**, *11*, e1001577. [CrossRef] [PubMed]